PROCEEDINGS, 43rd Workshop on Geothermal Reservoir Engineering
Stanford University, Stanford, California, February 12-14, 2018
SGP-TR-213

The Effects of Stimulation Process Conditions on the Thermal Performance of an Engineered Geothermal Reservoir

Mohammed G. ALHASHIM, Thanh Tung LE and Donald L. KOCH

Robert Fredrick School of Chemical and Biomolecular Engineering, Cornell University,

250 Olin Hall, Ithaca, NY, 14853

E-mail: dlk15@cornell.edu

Keywords: Rock stimulation, Hydroshear, Viscous flow, Hot dry rock, Thermal performance.

ABSTRACT

Engineered geothermal reservoirs are defined as low permeability hot dry rocks that are stimulated via the injection of a high pressure fluid. During the stimulation process, sealed weak planes are fractured forming a cluster of connected activated fractures. A weak plane is assumed to activate when the fluid pressure inside it reaches a critical value. The interconnectivity of the cluster of activated fractures varies depending on the importance of the viscous pressure drop when compared to the variability in the fracture's critical pressures. A well-connected cluster can form when the viscous pressure drop dominates while a fractal network is formed when the viscous pressure drop is negligible. Assuming one-dimensional heat transfer into the rock adjacent to each fracture and neglecting the interference between neighboring activated fractures, the circulation process within clusters of activated fractures, formed at different stimulation conditions, is analyzed. It is found that for the same ratio of the separation between the circulating wells to the cluster's radius, a well-connected cluster performs better than a fractal network. In the well-connected network, multiple flow paths connecting the two circulating wells are created while a fractal network provides a single flow path. For the well-connected network, the length of shortest path is on the order of magnitude of the Euclidean distance between the two wells providing a small surface area for thermal exchange. On the other hand, the shortest path of the fractal network is highly tortuous and its length is much greater than the separation distance between the two wells. Nevertheless, increasing the number of flow paths by a viscous-dominated fracturing process increases the thermal exchange between the cluster's longer paths and the shortest one. Additionally, it decreases the flow rate within each path leading to a net increase in the average residence time within the shortest path and better thermal performance.

1. INTRODUCTION

The goal of geothermal systems is to extract the thermal energy stored within rocks. Depending on the temperature of the rock, the extracted energy can be either used to generate electricity or/and can be used for heating applications. Ideal geothermal sites such as the ones found in Iceland and Turkey are composed of a porous layer with a high permeability that is near the surface and contains water as steam. These sites are typically denoted as hydrothermal rocks and are typically found near volcanoes (Sener et. al., 2000, Arnorsson, 1995). Such reservoirs are not abundant and extracting the stored thermal energy at other locations requires drilling to a deeper stratum where the temperature is sufficient for the desired application. If the permeability at the required depth is low, stimulation by injection of a high-pressure fluid is used to create a network of flow paths for the circulated fluid. Such systems are denoted as engineered geothermal systems (EGS) and their performance depends strongly on the connectivity of the formed network (Willis-Richards et. al., 1996, Fairley and Hinds, 2004).

Fluid transport during the stimulation process can lead to the creation of distinct network topologies that in turns affect the thermal performance of EGS. In this paper, we elucidate the effects of the network's connectivity induced by the fracturing process on the thermal performance of EGS by identifying the generated flow paths and quantifying their individual contribution to the thermal drawdown over a typical lifetime of EGS. We use a simple model that captures the effects of the fluid transport on the connectivity of a cluster of activated fractures to create networks at different process conditions. Then, we analyze their thermal performance by solving for the production temperature after a certain period of circulation.

The model assumes that the rock layer of interest contains many pre-existing fractures that form a network whose correlation length is on the order of the fractures' average length. When a high-pressure fluid is injected, these fractures slip and thus create flow paths for the circulating fluid. The slippage mechanism follows Mohr's criterion which yields a critical fluid pressure the fracturing fluid must reach to activate the fractures (Megel, 2007). The value of the critical pressure depends on the fracture orientation with respect to the in-situ stress field. Stress perturbations due to slippage are ignored and slippage occurs when the fracturing fluid reaches the fracture at a pressure that is higher than its critical pressure. After the stimulation process, a production well is drilled to intersect the network of activated fractures. Using the same injection well employed for stimulation, a low viscosity fluid is injected at a lower pressure than the fluid pressure used in the stimulation. We will assume that no fractures are activated during the circulation process. As the circulating fluid flows within the network of activated fractures, heat is conducted from the rock matrix to the fluid within the activated fractures. Thermal interference between the fractures is ignored and heat conduction in the flow direction is ignored.

The paper is organized as follows. In section 2, we first briefly describe the stimulation model that was used to generate networks of activated fractures at different process conditions. In section 3, we describe the heat transfer model that was used to calculate the production temperature after a certain period of circulation for the reservoirs generated using the model described in section 2. Then, we

analyze the thermal performance of an ensemble of reservoirs that are fractured under the same conditions in section 4. In the analysis, we identify the critical parameters that affect the thermal performance the most and analyze how the fracturing conditions alter such parameters.

2. RERSERVOIR STIMULATION MODEL

In this section, we describe the model used to create networks of activated fractures to analyze the thermal performance of stimulated rocks at different process conditions. The model captures the effects of fluid transport on the connectivity of the created cluster of activated fractures. Since the scope of the paper is the thermal performance of the created clusters of activated fractures and not the behavior of a growing cluster of activated fractures, we will briefly discuss the cluster's topology in different growth regimes without presenting the full analysis of the scaling laws that govern the cluster growth in such regimes.

Many hot dry rocks are developed via the stimulation of a nearly impermeable rock layer that contains an interconnected network of pre-existing sealed natural fractures. Upon fluid injection, these sealed natural fractures are hydrosheared leading to their activation. Once a fracture is activated, fluid filling volume is created that allows for fluid flow (Bruel, 2007; Kohl and Megel, 2007). Depending on the orientation of these natural fractures with respect to the in-situ stress field, they hydroshear at different fluid pressures. According to Mohr's law, a natural fracture is sheared when the fluid pressure within the fracture reaches a critical value such that the effective frictional force becomes equal or less than the shear stress acting on the fracture's surface. This critical value is a function of the fractures orientation with respect to the in-situ stress as (Wang, 1979):

$$P_c = \sigma_n - \tau/\eta \tag{1}$$

where σ_n and τ are the normal and shear stresses acting on the fracture's surfaces, respectively, and η is the friction coefficient.

Hence, the fracture can be activated due to different mechanisms by either perturbing the stress field around the fracture or perturbing the fluid pressure within the fracture. The activation of a natural fracture can lead to the creation of an excess shear stress on the neighboring fractures, thus lowering their critical pressure needed for slippage. This mechanism does not necessarily create a connected network of activated fractures. On the other hand, when the rock is saturated with a low viscosity fluid when compared to the viscosity of the fracturing fluid, the fluid pressure within the natural fractures is perturbed when the fracturing fluid reaches these fractures. Activating natural fractures via this mechanism ensures the creation of a connected network. In this paper, we neglect the effects of stress perturbations on the activation process and focus on the effects of fluid transport which lead to the creation of a connected network of activated fractures that can be used in the circulation process post stimulation.

To capture the effects of the viscous pressure flow on the growth of an activated fracture as fluid is injected, a simple model was used to model the effects of pressure driven flow on fracture propagation. In this model, a fracture is activated as slippage between the fracture's surfaces occurs following Mohr's criterion given by (1). Fluid filling volume is created due to the mismatch between the asperities of the fracture's surfaces upon their slippage. The fracture is initially saturated with a fluid with a viscosity that is much smaller than the fracturing fluid's. Hence, the region past the fluid front within the fracture does not meet Mohr's criterion, ignoring the effects of stress perturbations that result from the slippage of the fracture's surfaces, as the pressure within this region is smaller than the critical pressure required for slippage. Therefore, the fracture tip is assumed to be located at the fluid front and the volume of the activated portion of the fracture is assumed to be equal to the volume of the fluid flowing through the fracture. The geometry of the fracture is assumed to be rectangular with a width that is much larger than its length and aperture.

The fracture's aperture is assumed not to be affected by the fluid pressure within the fracture. This assumption ignores the effects of shear dilation that might increase the fracture's aperture (Rahman et. al., 2002) and it holds when the shear stiffness of the fracture is much larger than the characteristic pressure drop required to drive the flow of the fracturing fluid. Furthermore, all the fractures are assumed to have the same aperture in order to probe the effects of the path tortuosity and its length without the need to correct for its hydraulic conductance. Assuming the rock is impermeable, fluid loss from the fracture to the rock matrix is ignored. This assumption is valid when the time it takes to completely activate a fracture is much smaller than the time it takes to grow the cluster of activated fractures to a characteristic size where leakage starts to play a role in slowing down the growth of the cluster of the fractures.

In order to neglect the effects of the inherent interconnectivity of the pre-existing natural fractures, we assumed that the natural fractures form a well-connected network. This assumption applies when the number density of the natural fractures is large such that the network of pre-existing fractures looks homogenous at all length scales. Moreover, the critical pressures to activate the fractures are assumed to be uncorrelated with their orientation with respect to the in-situ stress field. This assumption applies when the in-situ stress is heterogeneous at large length scales and/or their friction coefficient are different. One can then assume that the pre-existing fractures form a network that we will approximate as a square lattice, where the critical pressures are statistically homogenous and are given by a probability density function, e.g. normal distribution.

Based on the above assumptions, the governing equation of the fluid front propagation within an activated rectangular fracture is given by:

$$\frac{d\lambda_i}{dt} = \frac{q_i}{bH}, \tag{2}$$

where b and H are the fracture's aperture and width, respectively. $\lambda_i(t)$ is the length of the propagating fracture and q_i is the volumetric flux within the activated fracture. The initial condition is $\lambda_i(t) = 0$. If leakage is negligible, the local mass balance within the fracture for a Newtonian fluid can be given by:

$$\frac{\partial^2 P}{\partial x^2} = 0. \tag{3}$$

(3) assumes that the fluid flow within the planer fractures follows the cubic law where $q_i = \frac{b^3 H}{12\mu}\frac{\partial P}{\partial x}$ (Zimmerman and Bodvarsson, 1996). At the injection node, a constant injection rate, Q is assumed that is equal to the sum of the flux in the set of activated fractures, S_{inj}, intersected by the injection well, i.e. $\sum_{i \in S_{inj}} q_i = Q$.

Since slippage of the fracture's surface requires that the fluid pressure must be at least equal to the critical pressure, one can set the fluid pressure at the fluid front within each growing fracture to be equal to the fracture's critical pressure, P_{c_i}, i.e. $P(\lambda_i, t) = P_{c_i}$. Using Euler integration scheme, we solve for the time dependent length of the fracture using (2) after solving for the fluid pressure at all junctions to calculate q_i. To solve for the fluid pressure at all junctions, a linear system of equations can be used:

$$A_{ij} p_j = B_i, \tag{4}$$

where A is the coefficient matrix that contains information about the connectivity of the activated fractures and their lengths, p is the fluid pressure at the junctions and B is a vector that specifies the boundary conditions. A constant injection rate, Q, was used as a boundary condition at the injection well.

(4) applies a mass balance at each junction where the flux within a partially activated fracture is driven by the pressure drop $p_j - P_{c\,jk}$ where p_j is the fluid pressure at the junction j and $P_{c\,jk}$ is the critical pressure to activate a fracture that connects the two nodes j and k. For a fracture that is completely activated, i.e. its fracture tip has reached junction k, fluid flow within a fracture jk is driven by the pressure drop between the two nodes ($p_j - p_k$).

By using the standard deviation of the critical pressures, δ_{pc}, as a characteristic fluid pressure, the length of the pre-existing fractures, l, as the characteristic length scale and $\frac{bHl}{Q}$ as the characteristic time, one can derive a dimensionless number, $F_N \equiv \frac{\delta_{pc} b^3 H}{12\mu Q l}$ where μ is the fracturing fluid viscosity, that captures the importance of the characteristic viscous pressure drop within a fracture when compared to the variability in the critical pressures. This dimensionless number is related to the characteristic correlation length, ξ_{ch}, of the cluster of activated fractures through, $\xi_{ch} = k_\xi \xi_0 F_N^{\frac{\nu}{\epsilon+1}}$. ξ_0 is the correlation length of the network of pre-existing fractures. In the case of a perfect square lattice of bonds, ξ_0 is equal to the lattice spacing l. ν is a universal exponent that captures the scaling of the correlation length with the distance of a percolating parameter, such as the fluid pressure for instance, from a threshold value. It depends on the dimension of the network and for a two-dimensional network, it is equal to 4/3. ϵ is the scaling exponent for the effective permeability of the cluster of activated fractures and is approximately equal to 1.3 for a two-dimensional network. Finally, k_ξ is a proportionality constant that is of order one and depends on the geometry of the network of pre-existing fractures. Derivation of the relationship between the cluster's correlation length and the dimensionless number F_N comes from applying percolation theory to analyze the growth of a cluster of activated fractures when pressure-driven flow drives the growth dynamics. Details of the theory will be published elsewhere.

The connectivity of the network of activated fractures depends on the relative value of ξ_{ch} when compared to the correlation length of the pre-existing fractures and the radius of the cluster of activated fractures, R. Depending on the value of F_N and thus ξ_{ch}, the fracturing process can either be controlled by the viscous dissipation of the fluid or the range of resistances the fluid has to overcome in order to form percolating paths within the stimulated rock. If $\xi_0 \ll R \ll \xi_{ch}$, the viscous pressure drop is negligible over the length scale of the cluster's radius and the fluid activates the smallest resistance available. In this regime, a fractal network is formed where the structure of the cluster is equivalent to a percolating network formed at the threshold value. The fractal dimension of the network is equal to 1.9 in two dimensions and the network's properties scale with the length scale used to analyze the network. For example, the permeability, K, of the fractal network depends on the length scale at which a pressure drop is applied, i.e. $K \sim d^\epsilon$ where d is the length scale of interest. Another property that is relevant to the analysis of the thermal performance of a cluster of activated fractures is the length of the shortest path between two points within the network. The length of the shortest path, L_s, between two points within the fractal network scales with the Euclidean distance, d, between the two points as $\frac{L_s}{l} \sim \left(\frac{d}{l}\right)^{d_{min}}$ where $d_{min} \approx 1.13$ for a two dimensional network (Zhou et. al. 2012). In fact, for an infinite fractal network, there is only one path connecting two points within the network whose length is given by the scaling of L_s. Throughout this paper, we will refer to the fractal regime when we analyzed the thermal performance of reservoirs that are stimulated under conditions where the viscous pressure drop is negligible over the length scale of the cluster's radius.

Moreover, in the regime where the viscous pressure drop is important over the length of the pre-existing fractures, l, the fracturing fluid easily overcomes the critical pressures of the natural fractures. This regime, denoted as the homogenous regime, applies when $\xi_0 \sim \xi_{ch} \ll R$. The formed network is well-connected and it looks homogenous at all length scales, i.e. its fractal dimension is equal to the dimension of the network. In this regime, the average separation of between the activated fractures is of the same order of magnitude as the average separation of the pre-existing natural fractures. The cluster of activated fractures can be described as an effective continuum medium where its properties are homogenous everywhere and do not change with the length scale of interest. For example, the permeability of the network is given by $K \sim \frac{b^3}{l}$. The shortest path between two points within the network in this regime is of the same order of magnitude as the Euclidean distance such that $L_s \sim d$ and there exists an infinite number of paths connecting the two points when the size of the network is infinity.

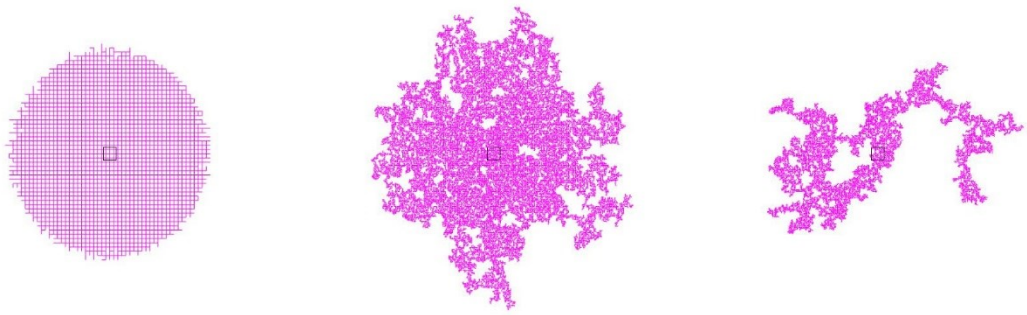

Figure 1: Example of networks stimulated in the three different regimes. Figure 1a shows a network that is activated for $F_N = 0.005$ representing the homogenous regime. Figure 1b shows a network that is activated at $F_N = 15$ and figure 1c shows a network that is formed when $F_N = 2000$ where the fractal regime is reached.

Between the fractal and homogenous regimes, there is an intermediate regime where the network's properties depend on the length scale of interest and the characteristic correlation length, ξ_{ch}, of the cluster of activated fractures. In this regime, the viscous pressure drop is negligible over ξ_{ch}but is important on the scale of the cluster radius, R. The cluster of activated fractures looks fractal at length scales that are smaller than ξ_{ch} but is heterogeneous, due to the viscous pressure drop, on the scale of the cluster radius. The activation process over a length scale that is much smaller than ξ_{ch} but much larger than ξ_0 is governed by the same rules used to generate a percolating network near the percolation threshold. Over a length scale that is much larger than ξ_{ch}, the network can be approximated as an effective continuum medium where its local properties scale with the local correlation length, ξ_l, of the cluster of activated fractures. ξ_l varies spatially with the network and it is a function of the local fluid pressure during the stimulation process. For this regime to fully develop, $\xi_0 \ll \xi_{ch} \ll R$ and the length of the shortest path between two points that are separated by a distance d that is much smaller than ξ_l will scale as $l\left(\frac{d}{l}\right)^{d_{min}}$ (Dokholyan et. al., 1999). However, the scaling of L_s when d is much larger than ξ_{ch} is a function of d, R and the local correlation length; i.e. $L_s \sim cd\left(\frac{\xi_{ch}}{l}\right)^{d_{min}-1}$ where c is a pre-factor that is a function of $\frac{d}{R}$. Derivation of this scaling comes from analyzing the growth of the cluster of activated fractures in this regime using percolation theory. It is worth mentioning that in each of these three regimes, the structure of the network is self-similar. The size dependence of the network structure only arises during the transitions between the regimes.

To illustrate the network structure in the three regimes, we simulated the fracturing process at different values of F_N and plotted the structure of the network in figure 1. As can be seen in the figure, there are no fractures in the interior of the cluster that are not activated when the network is stimulated in the homogenous regime. As mentioned before, as the viscous pressure drop becomes dominant over the variability in the critical pressures, the fluid easily overcomes the resistance to activate the fractures that are connected with the percolating network through which the fracturing fluid flows. Once the fluid front reaches a natural fracture, it is activated forming a network with homogenous properties, as shown in figure 1a, that are equal everywhere within the network. As the viscous pressure drop decreases and becomes negligible over the length scale of ξ_{ch}, the network is nearly fractal at small length scales but is heterogeneous over the length scale of the cluster radius as shown in figure 1b. Finally, when F_N is too large such that $\xi_{ch} \gg R$, the network looks fractal at all length scales as shown in figure 1c.

The thermal performance of an engineered geothermal system depends on the connectivity of the network and the positioning of the production well. As shown in figure 1, the relative magnitude of the viscous pressure drop and the variability in the critical pressures during the stimulation process can lead to a wide range of network connectivities ranging from a well-connected network to a fractal one. If the interference between the activated fractures is neglected, it can be easily seen that one needs to activate all available pre-exsiting fractures to create a high surface area for heat exchange and reduce the impedance of the network due to the creation of many paths connecting the two wells. To increase the residence time within the network, one can position the production well at the edge of the cluster of activated fractures. Based on this model, one can set the stimulation process conditions such that F_N approaches zero, in order create a well-connected network of activated fractures. Due to the uncertainty in the statistical information of the rocks such as the aperture of the fractures, their orientation distribution and the value of the principal stress field using current tools, it is still a difficult task to accurately tune the value of F_N. Hence, geothermal reservoirs are most likely stimulated at a wide range of values of F_N. In fact, Sahimi (2011) has argued that all networks of activated fractures are either fractal or are fractal at small length scales but homogenous at large length scales. For example, the Gyesters geothermal reservoir in California has been found to form a fractal network of activated fractures (Tayeb et al. 2011). This corresponds to the range of values for F_N that is much larger than the fracture spacing between the pre-existing fractures, i.e. $\xi_{ch} \gg R$. Using the present model, the critical structural features of the network of activated fractures that affect the thermal performance the most will be identified and the manner in which such features are affected by the viscous pressure drop during the stimulation process will be discussed.

3. HYDROTHERMAL MODEL

To model the circulation process, we have adopted the exact solution for the production temperature derived by Fox et al.(2016). In this section, we first summarize the major assumptions of the model. We then discuss simple cases that illustrate the physical features of the

model. Finally, we give the procedure for applying the model to simulate the circulation process for the clusters of activated fractures created using the stimulation model discussed in the previous section.

The major assumptions of the model are as follows: the heat transfer between the circulating fluid and the rock matrix is assumed to be dominated by one-dimensional heat conduction and is coupled with heat convection within the circulating fluid. Heat transfer due the temperature gradient along the direction of the flow is neglected. Moreover, the interaction between the neighboring fractures are assumed to be negligible because the penetration length of the conducted heat within the rock matrix is much smaller than the fracture separation. Finally, the activation of sealed fractures during the circulation process is ignored. Based on these assumption, Fox et al.(2016) derived an exact expression for the production temperature, θ_p, of a discrete network of active fractures given information about the flow paths between the injection and production wells. θ_p is given by:

$$\theta_p = 1 - \sum_k^{n_p} C_k. \tag{5}$$

$\theta_p \equiv \frac{T_p - T_{inj}}{T_r - T_{inj}}$ where T_p is the production temperature, T_{inj} is the temperature of the injected fluid and T_r is the far-field temperature of the rock matrix. n_p is the number of flow paths connecting the production and injection wells and C_k is the contribution of a flow path k to the thermal drawdown after a certain period of circulation which is given by:

$$C_k = M_k \operatorname{erfc}\left[\frac{\beta l}{\sqrt{\alpha t}} \sum_{j \in S_k} \frac{1}{f_j}\right], \tag{6}$$

where f_j is the fraction of the injected fluid flowing within segment j that belongs to the path set S_k. $M_k = \prod_{j \in S_k} \chi_j$ where χ_j is a function of the connectivity of the path segments with other paths. The value of χ_j for segment j is equal to the ratio of the fluid flow within segment j to the sum of the fluid flow of the other segments connected at the downstream junction of these segments. β is a dimensionless parameter and is defined as $\beta \equiv \frac{2Hk_r}{Q\rho_f c_{p_f}}$ while $\alpha \equiv \frac{k_r}{\rho_r c_{p_r}}$ is the thermal diffusivity of the rock. k_r is the rock's conductivity. ρ_f and c_{p_f} are the circulating fluid's density and specific heat capacity, respectively. ρ_r and c_{p_r} are the density and heat capacity of the rock matrix, respectively. Q is the injection rate of the circulated fluid.

A major advantage of the model is that one can explicitly quantify the contribution of participating flow paths, C_k, on the thermal drawdown. Hence, one can compare the effects of paths with distinct properties such as their length and average flow within each path on the thermal performance. As can be seen from (6), the contribution of the individual path to decreasing the production temperature, T_p, depends on the residence time of the circulating fluid within the segments constituting the path, and the degree of thermal exchange between the fluid flowing within a path with the fluid coming from other paths. The degree of thermal exchange is depicted by the multiplicative term M_k which can be defined as the ratio of the path's contribution to the contribution it would have if there was no mixing between the paths. Increasing the degree of interaction decreases the value of M_k and if there is no mixing, $M_k = 1$. To elucidate the physical mechanisms by which these parameters affect the thermal drawdown of an arbitrary path k, we will explore extreme cases where (6) can be simplified.

Consider the simplest case where there exists only one path connecting the two wells. This case applies when an infinite cluster of activated fractures is fractal. In this case, the contribution of the path to the thermal drawdown is simply given by $C_k = \operatorname{erfc}\left[\frac{\beta L_1}{\sqrt{\alpha t}}\right]$ where L_1 is the total length of the only path connecting the two wells. In this case, $f_j = 1$ and $M_k = 1$ since all the circulating fluid flows through this path. As can be seen, the thermal drawdown of the path depends on its length and the injection rate of the circulating fluid. Decreasing the residence time by increasing the injection rate for example shortens the lifetime of the reservoir.

Now, consider a more complex but tractable case. When the two wells are connected via multiple paths that are parallel to each other, (6) reduces to:

$$C_k = \langle f_j \rangle_k \operatorname{erfc}\left[\frac{\beta}{\sqrt{\alpha t}} \frac{L_k}{\langle f_j \rangle_k}\right], \tag{7}$$

where $\langle f_j \rangle_k$ is the average fraction of the injected fluid flowing within the path and in this case, the flow within each segment constituting the path is equal to the average value. Similar to the single path case, the contribution to the thermal drawdown depends on the average residence time within the path. Moreover, the degree of interaction in this case is inversely proportional to the average flow rate within the path. As the fluids coming from different paths add up at the production well, the effects of the paths with the lowest flow rate on the production temperature will be small compared to other paths.

By applying a mass balance at the production well for the parallel path model, $Q = \sum_k^{np} q_k$ where q_k is the flow rate within path k. From the definition of χ_j, its value for all the fractures within the path is equal to 1 except for the fracture that is intersected by the production well. The value of χ_j for this fracture is given by $\frac{q_k}{Q}$ and thus $M_k = 1 \cdot 1 \cdot 1 \cdots \frac{q_k}{Q} = \langle f_j \rangle_k$. In contrast to the single path case where $\langle f_j \rangle_k$ is independent of the length of the path when the injection rate is fixed, the average flow within a path for the parallel paths' case decreases when the length of the path and the network's connectivity increases. In fact, $\langle f_j \rangle_k = \frac{b^3 H}{12\mu} \frac{Z}{L_k}$ where Z is the impedance of the network. The impedance of the network is a measure of the required pressure drop across the network, ΔP, to drive the flow of the

circulating fluid and is defined as $Z \equiv \frac{\Delta P}{Q}$. Since the average viscous flow within path k is given by $q_k = \frac{b^3 H}{12\mu}\frac{\Delta P}{L_k}$ when the aperture and width of the fractures are the same, one can show that $\langle f_j \rangle_k = \frac{b^3 H}{12\mu}\frac{Z}{L_k}$.

To see how the connectivity of the network affects the average flow within the path, consider how Z changes with the number of paths. By substituting the average viscous flow relation, q_k, and the definition of Z in the mass balance over the production well, one can find that $Z \sim \frac{1}{\sum_k^{n_p} \frac{1}{L_k}}$. As the number of paths available for the fluid to flow through increases, the resistance within the network decreases due to the increase in the options for the fluid to flow through. Hence, the average flow within each path decreases. Moreover, $\langle f_j \rangle_k$ increases as the length of the other paths connecting the two wells increases.

Although the dependence of $\langle f_j \rangle_k$ on the number of flow paths and the path's length is derived for the case of parallel paths, it applies for a network where the paths are interconnected, i.e. $\langle f_j \rangle_k \sim \frac{Z}{L_k}$. As the network becomes well-connected, the number of paths connecting the two wells increases which in turn reduces the impedance of the network. In the case of interconnected networks, the contribution of an arbitrary path to the thermal drawdown can be approximated as $C_k \approx M_k \mathrm{erfc}\left[\frac{\beta}{\sqrt{\alpha t}}\frac{L_k}{\langle f_j \rangle_k}\right]$. The value of M_k is difficult to approximate for interconnected networks as it depends on how the path of interest is intersected by another path. Figure 1A in the appendix shows a simple example of two intersecting paths and how M_k depends on the nature of intersection.

Based on the above analysis, one can see that the dependence of the thermal performance on the stimulation conditions will depend on the way the value of F_N affects the length of the paths and their interconnectivity measured by the impedance of the formed network. Now, let us briefly describe the method used to simulate the circulation process after forming a cluster of activated fractures using the model described in section 2. The hydrothermal simulation of the circulation process consists of four main steps: 1) placement of the production well; 2) solving for the fluid flow within the network; 3) determining the flow paths connecting the injection and production wells; and 4) calculating the production temperature after a certain period of circulation by numerically solving (6).

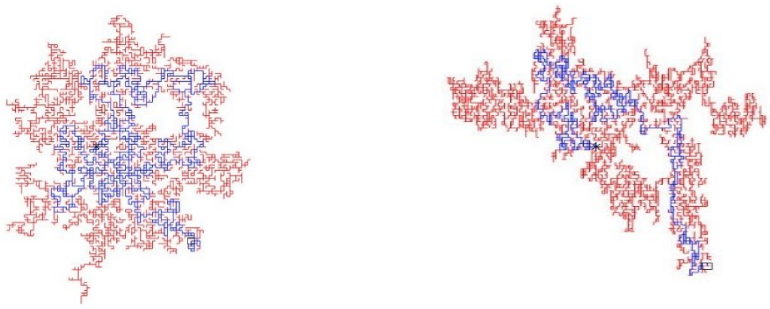

Figure 2: Example of clusters stimulated at different values of F_N. The production well is placed at a distance $d = 0.8R$. Figure 2a shows a network stimulated at $F_N = 20$ while figure 2b shows a network stimulated at $F_N = 2000$. Red fractures are dead-ends while the blue ones carry the fluid. As can be seen, as the network becomes sparser, the fraction of the dead end fractures increases.

In the first step, the injection node used in the stimulation process is also used as an injection well for the circulation process. For a specific well separation, d, a random node within the cluster, located at a distance d from the injection node, is chosen as the production well. The choice of the production well's position determines the flow paths between the two wells since not all the fractures, for a sparse network, will carry the fluid during the circulation process. Figure 2 shows examples of clusters of activated fractures formed at different values of F_N where the production well is placed at a distance d such that d/R is equal to 0.8 where R is the extent of the cluster from the injection well. The red segments represent the dead end fractures that will not participate in the heat transfer during the stimulation process since fluid flow within them is zero while the blue bonds represent the activated fractures that will carry out fluid during the circulation process. The asterisk symbol represents the position of the injection well and the square symbol represents the position of the production well. As the network becomes sparser, the flow structure becomes more sensitive to the placement of the production well since there are many fractures that are not well connected with other activated fractures. For a well-connected network, stimulated at small F_N, the sensitivity of the flow structure to the position of the production well is weak and the number of dead-end fractures is small. Finally, due to the viscous pressure drop, the connectivity of the network varies locally. Thus, the further away the production well is placed, the more likely it will fail to intersect the network of activated fractures.

Since the heat conduction within the circulating fluid is neglected, fluid flow can be solved as a separate problem from the heat transfer one where the flux within the fractures become an input to solve (6). To determine q_j for all fractures within the network, a linear system of equations, for the pressure at the junctions, similar to that used to solve for the fluid flow during the stimulation process is used but with different boundary conditions. The boundary conditions in this case are the pressure, P_{inj}, at the injection well and the

production flow rate at the production well. For more details on the algorithm used to solve for the system of equations, the reader is referred to Fox et al.(2016).

In the third step, we used a recursive depth-first method to identify the flow paths between the two wells. This method requires a large memory because the matrix used to identify the paths grows as one traverses through the network using a recursive function, so we limited the path search to the ones that significantly contribute to the thermal drawdown after the specified period of circulation and omit the ones that have a negligible contribution. A criterion based on (6) was used to stop the search for a particular path when the term within the complementary error function, $\frac{\beta l}{\sqrt{\alpha t}}\sum_{j\in S_k}\frac{1}{f_j}$, becomes larger than 2.5; an arbitrary value that was chosen such that the error introduced by this approximation is less than 0.1%. Not only did this method reduce the memory requirement to find the paths to be used in solving for the production temperature, but it also sped up the simulation since most lengthy paths will not be searched as $\frac{\beta l}{\sqrt{\alpha t}}\sum_{j\in S_k}\frac{1}{f_j}$ becomes larger as the length of the path increases. Nevertheless, the search algorithm is slow for simulating the large clusters of activated fractures needed to avoid finite size effects.

Finally, after identifying the paths that contribute to the thermal drawdown, the production temperature of the circulated fluid is calculated at different times and compared for different network topologies produced via the stimulation model. In the next section, we show that the length of the shortest path and the average flow within it are the most important parameters to determine the thermal performance of a network. By identifying their dependence on the process conditions at which the network is stimulated, one can correlate the thermal performance of a network with the value of F_N.

4. RESULTS AND DISCUSSION

In section 2, it was shown that the importance of the viscous pressure drop when compared to the variability in the critical pressures lead to distinct network topologies. The cluster's correlation length, ξ_{ch}, over which the viscous pressure drop is important depends on the properties of the fracturing fluid, the injection rate, and some physical properties of the rock such as the variability in the critical pressures of the natural fractures, their length and aperture. Depending on the value of ξ_{ch} compared to the cluster's radius, R, three growth regimes where the network's properties scale differently are identified. In the homogenous regime where $\xi_0 \sim \xi_{ch} \ll R$, a well-connected network is formed where all the natural fractures are activated when the fluid front reaches them. Moreover, a fractal cluster of activated fractures was shown to form in the fractal regime when $\xi_0 \ll R \ll \xi_{ch}$ where the fractal dimension of the network is the same as the fractal dimension of a percolating network formed at the threshold value. Finally, a nearly fractal network is formed in the intermediate regime when $\xi_0 \ll \xi_{ch} \ll R$ where the connectivity of the network mainly depends on the value of ξ_{ch}. In this section, we show how the thermal performance varies with ξ_{ch} in the three regimes. In particular, we identify the important parameters that affect the thermal performance and are functions of the fracturing process protocol.

To assess how the thermal performance varies with ξ_{ch}, we stimulated the rock at different values of F_N for a specific amount of fluid injected at a constant rate for a certain period of time; a typical strategy used in the stimulation process. We have considered two cases where the injected amount is different. In case I, 900 m^3 of the fracturing fluid is injected while 600 m^3 is used to stimulate the rock in case II. In both cases, the dimensions of the activated fractures are those listed in table 1A in the appendix. Such values were chosen to keep the calculations fast enough while producing large enough clusters to probe the three growth regimes. Varying the value of F_N can represent either using different viscosities for the fracturing fluid, injecting the fluid at different rates, or using the same fracturing fluid injected at the same rate for different rocks with various statistical properties of the natural fractures. A large square grid representing the network of natural fractures was used where the critical pressures for the natural fractures are randomly drawn from a normal distribution. The size of the square grid is arbitrary and is chosen such that the fracturing fluid does not reach the grid's boundaries during the stimulation process. The stimulation process is stopped when a certain number of activated fractures are formed to keep the total volume of the injected fluid the same for all cases. Then, a production well is placed at a distance d from the injection well such that $\frac{d}{R} = 0.8$ where R is the furthest extent of the front of the fracturing fluid. The value of R represents the position of the front of the resulting micro seismic cloud formed during the fracturing process. For each value of F_N, all the properties of the network and the corresponding thermal performance parameters were averaged over 2000 realizations.

Before introducing the trend of the production temperature after ten years of circulation for both cases, let us see how the size and connectivity of the cluster of activated fractures change with the stimulation conditions. Figure 3a shows the average radius of the cluster of activated fractures, R, for different values of F_N, represented by the ratio of the correlation length of the cluster of activated fractures, ξ_{ch}, to R. The blue curve represents case I where 900 m^3 of the fracturing fluid is injected to stimulate the rock while the red curve represents case II where 600 m^3 is injected. In general, as the viscous pressure drop becomes important when compared to the variability in the critical pressures, the size of the cluster of activated fractures decreases. When the fluid's pressure increases to drive the flow, it activates more fractures near the injection well. Hence, the amount of fluid available to extend the radial extent of the cluster decreases. Intuitively, the more fluid is injected underground, the larger the cluster is by comparing R for cases I and II for the same value of F_N. Furthermore, the radius of the cluster is independent of the value of F_N in the homogenous and fractal regimes while it increases with F_N in the intermediate regime. In the homogenous regime, i.e. $\xi_0 \sim \xi_{ch}$, the viscous pressure drop is dominant over the length scale of the fractures' length, l, and therefore the fracturing fluid activates all fractures it encounters regardless of the range of resistances to activate the natural fractures. In contrast, the viscous pressure drop is negligible in the fractal regime, i.e. $\frac{\xi_{ch}}{R} \gg 1$, and the injected fluid is only able to activate the fractures with the lowest critical pressures that are connected to the percolating path of the fluid. In between such regimes, the radius of the cluster increases with decreasing the viscous pressure drop as less fluid is used to activate fractures near the injection well as it becomes harder to overcome their critical pressures.

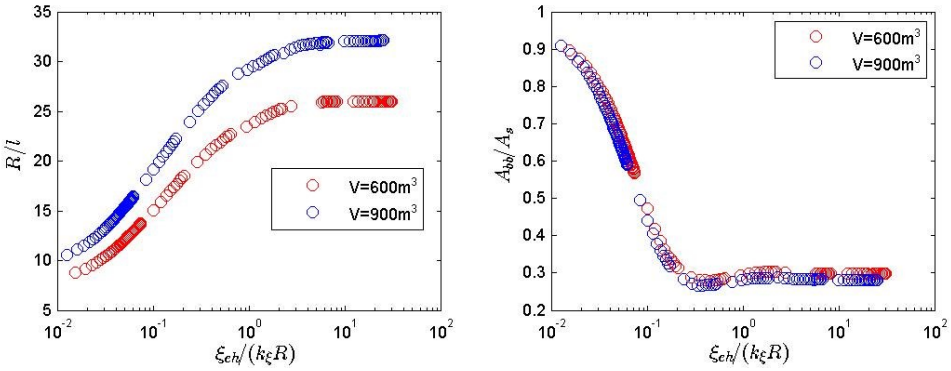

Figure 3: The size and connectivity of the network of activated fractures as a function of $\xi_{ch} = k_\xi \xi_0 F_N^{\frac{\nu}{\epsilon+1}}$. Figure 3a shows the maximum extent of the cluster of activated fractures from the injection well, R as a function of ξ_{ch}. Figure 3b shows the ratio of the surface area of the backbone fractures, which carries the circulated fluid, to the total surface area of the activated fractures. The blue curves correspond to the case of injecting 900 m^3 of water while the red curves correspond to the case of injecting a total amount of fluid of 600 m^3. As can be seen in the figures, increasing F_N and hence ξ_{ch} produces a larger but sparser network of activated fractures. Due to finite size effects, the two curves do not collapse completely.

The connectivity of the cluster of activated fractures can be depicted by the ratio of the surface area of the backbone fractures, A_{bb} to the total surface area of the activated fractures, A_s. The backbone fractures are the ones that carry the circulating fluid between the two wells and are represented by the blue links in figure 2. In the homogenous regime, all the activated fractures form paths between the two wells, i.e. $\frac{A_{bb}}{As} \to 1$ for infinite networks regardless of the position of the production well as shown in figure 3b.

In the intermediate regime where $\xi_0 \ll \xi_{ch} \ll R$, the fraction of activated fractures that belongs to the backbone of the cluster decreases as the cluster becomes sparser. Since the network in this regime is self-similar and we have fixed the ratio between the distance between the wells and the radius of the cluster, $\frac{A_{bb}}{As}$ does not depend on the size of the cluster as shown in the figure. Nevertheless, the network's connectivity depends on the location of the production well, i.e. the distance between the two wells, d. Since the connectivity of the network is heterogeneous as it depends on the local fluid pressure that varies spatially when the viscous pressure drop is important, the region far away from the injection well is sparser than the interior region of the cluster. Hence, as the distance between the two wells decreases, more of the fractures that are near the edge of the cluster will not participate in carrying the fluid.

When $\frac{\xi_{ch}}{R} \gg 1$, the activated natural fractures form a fractal network. In this regime, $\frac{A_{bb}}{A_s}$ becomes independent of F_N since the viscous pressure drop is negligible and does not control the fracturing process. Similar to the intermediate regime, the formed fractal network of activated fractures is self-similar at length scales smaller than the correlation length of the cluster and the connectivity depends on the separation distance between the two wells. In fact, $\frac{A_{bb}}{A_s} \to 0$ as $R \to \infty$ since $\frac{A_{bb}}{A_s} \sim d^{D_{bb}-D_f} \sim d^{-0.26}$ where D_{bb} is the fractal dimension of the backbone and is equal to $D_{bb} = 1.64$ while the fractal dimension of the whole cluster, D_f, is equal to 1.9.

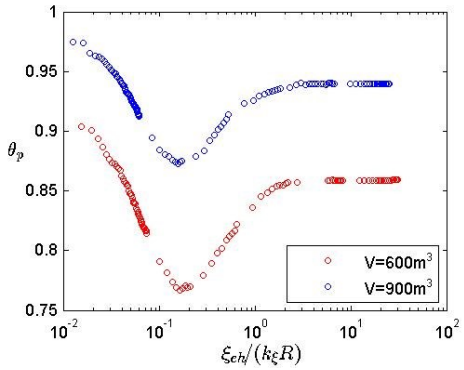

Figure 4: The dimensionless temperature of the produced water after ten years of circulating the fluid as a function of ξ_{ch}. As can be seen in the figure, stimulating a rock with a high viscosity fluid for example produces a well-connected network with the highest thermal performance. As the connectivity of the network decreases by increasing F_N, the thermal performance decreases reaching a minimum when the intermediate regime is approached. When the network becomes nearly fractal the thermal performance increases as the network becomes sparser. For fractal networks, the thermal performance becomes independent of F_N.

To probe the effects of the stimulation process on the thermal performance, we compared the dimensionless temperature, θ_p, of the produced fluid after ten years of circulation for networks fractured at different values of F_N. Table 1 in the appendix lists the parameters used to simulate the circulation process. Figure 4 shows the value of θ_p for different values of F_N. As shown in the figure, well-connected networks, formed in the homogenous regime, perform the best. As the intermediate regime is approached by increasing F_N, the thermal performance decreases. The intermediate regime is reached when $F_N \gg 1$ such that $\frac{\xi_{ch}}{\xi_0} \gg 1$ be satisfied. The minimum production temperature in figure 4 is located at $F_N = 8$ ($\frac{\xi_{ch}}{k_\xi R} \approx 0.2$). In the intermediate regime, $F_N > 8$, the thermal performance increases with F_N and it plateaus when the viscous pressure drop becomes negligible and the formed network becomes fractal.

As mentioned in section 3, the thermal performance depends on the interconnectivity, average flow, and length, of the paths connecting the two wells. It was shown that the competition between the length of the path and the average flow within it affects the path's contribution to the thermal drawdown. The average flow within a path was shown to depend on both the length of the path and the impedance of the network which decreases as the network becomes more interconnected. The length of the path depends on the distance between the two wells and it also increases as the network becomes sparser. One can explain the trend presented in figure 4 by considering the way the path properties change with F_N in the three regimes. Since the average flow and length is different for various paths, their contribution to the thermal drawdown will also be different. Some will contribute after 1 day of circulation for example while others will start to contribute after decades of circulation. In fact, each path will start to contribute when $\frac{\beta}{\sqrt{\alpha t}} \frac{L_k}{\langle f_j \rangle_k} \sim O(1)$. Since $\langle f_j \rangle_k \sim \frac{Z}{L_k}$, the shortest path is expected to be the earliest path to drive the thermal drawdown as the fluid is circulated.

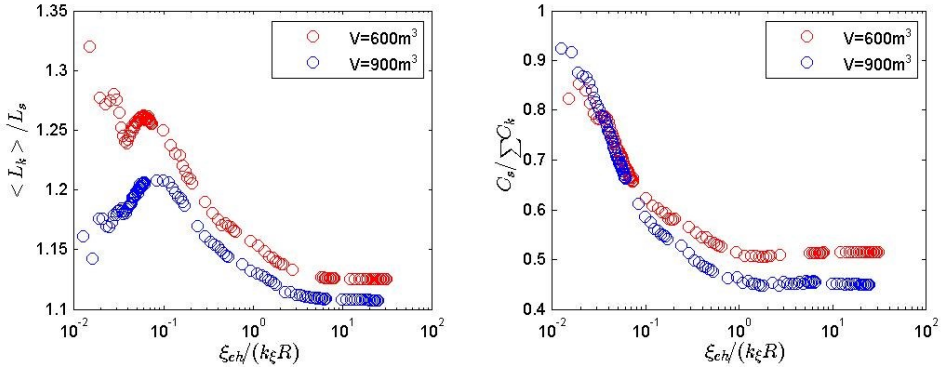

Figure 5: This plot is to show that the shortest path is the most important path in the drawdown on of the production temperature. Figure 5a shows the ratio of the average length of the paths that contribute in the temperature drawdown when compared to the length of the shortest path. For all values of F_N, the average length of the paths is of the same order of magnitude as the shortest path. Figure 5b shows the fraction of the contribution of the shortest path in the drawdown of the temperature. For almost all values of F_N, more than 40 percent of the thermal drawdown comes from the shortest path only. As F_N decreases and the average flow within the other paths increases, more paths start to contribute.

Figure 5a shows the average length of the paths, $\langle L_k \rangle$, that contribute to the thermal drawdown after ten years of circulation, normalized by the length of the shortest path, L_s. As can be seen in the figure, for all values of F_N, the average length of the contributing paths is of the same order of magnitude as the shortest path. One should note that as the intermediate regime is approached by increasing F_N, $\frac{\langle L_k \rangle}{L_s}$ increases and it decreases in the intermediate regime until the fractal regime is fully developed where $\frac{\langle L_k \rangle}{L_s}$ plateaus. This behavior will be explained more clearly when we discuss the effects of F_N on the properties of the shortest path later on. The general trend of $\frac{\langle L_k \rangle}{L_s}$ does not change with time but the absolute value increases with time as more paths begin to contribute during the lifetime of the reservoir.

Furthermore, we quantified the contribution of the shortest path, C_s, when compared to the total contribution to the thermal drawdown from all other paths, i.e $\sum_k^{n_p} C_k$, as shown in figure 5b. For all values of F_N, more than 40 percent of the thermal drawdown comes from the shortest path alone. The absolute value of $C_s / \sum_k^{n_p} C_k$ changes with time as more paths begins to contribute over the course of the lifetime of the geothermal reservoir. However, the trend of $C_s / \sum_k^{n_p} C_k$ for different values of F_N is expected to be the same since it depends on the structure of the network. In the homogenous regime, the number of paths connecting the two wells is large. However, few of the existing paths contribute to the thermal drawdown since $\frac{\beta}{\sqrt{\alpha t}} \frac{L_k}{\langle f_j \rangle_k}$ for most paths is much larger than one as $\langle f_j \rangle_k$ is expected to be small for a well-connected network. As the network becomes sparse, more paths start to contribute and the average flow within the paths increases thereby reducing the relative contribution of the shortest path. In the fractal regime, there exists only one path connecting the two wells for an infinite cluster of activated fractures. Hence, $C_s / \sum_k^{n_p} C_k$ is expected to be equal to one. However, we are

simulating small clusters where finite size effects are present. The number of paths connecting the two wells for a small cluster is finite and most of these paths contribute to the thermal drawdown since their length is of the same order of magnitude as the shortest path as shown in figure 5a. This reduces the relative contribution of the shortest path.

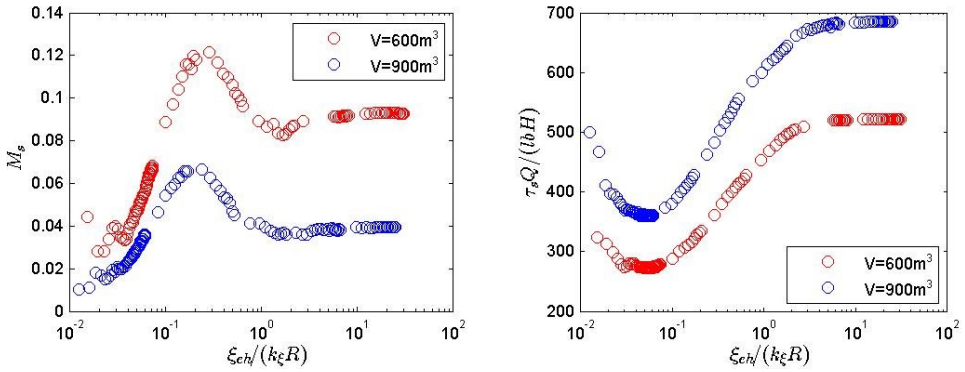

Figure 6: The critical properties of the shortest path that control the thermal performance as a function of the network's correlation length. Figure 6a shows the value of M_s whose inverse value can be interpreted as the degree of mixing between the fluid of the shortest path and other paths within the network while figure 6b shows the residence time of the fluid within the shortest path. The behavior of both properties as a function of F_N is different in the three regimes.

As mentioned in section 3, the contribution of an arbitrary path is $C_k \approx M_k \operatorname{erfc}\left[\frac{\beta}{\sqrt{\alpha t}}\frac{L_k}{\langle f_j\rangle_k}\right]$. Since it was found that the shortest path is the most important path in producing the thermal drawdown of the production temperature, the trend presented in figure 4 can be explained by analyzing the behavior of the fluid's residence time, $\tau_s = \frac{HbL_s}{Q\langle f_j\rangle_s}$, within the shortest path and the degree of thermal exchange (mixing), M_s^{-1}, between the shortest path and other paths within the network as F_N and the size of the network are varied. The multiplicative term, M_s, of the shortest path is a function of both the relative average flow within the shortest path to the average flow within the whole network and its interconnectivity with the other paths. Figure 6a shows a plot of M_s as a function of the network's correlation length normalized by the radius of the cluster for both cases I and II while figure 6b shows the behavior of τ_s in the three regimes. As can be seen in figure 6a, M_s increases as the intermediate regime is approached. Then, it decreases with F_N in the intermediate regime and levels off when the fractal regime is fully developed, i.e. $\xi_{ch} \gg R$. Similarly, the ratio of the average flow within the shortest path to its length increases as the network becomes sparser and it decreases when $\xi_0 \ll \xi_{ch} \ll R$. Then, it levels off when the cluster of activated fractures become fractal.

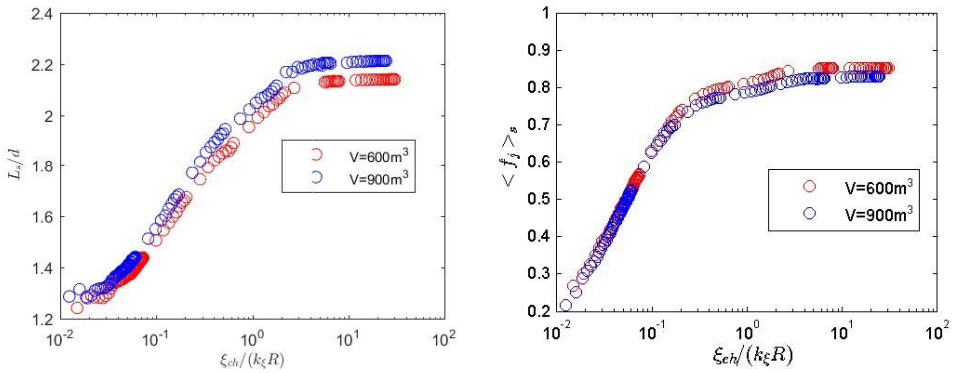

Figure 7: The tortuosity and average flow rate within the shortest path as a function of the characteristic correlation length. Figure 7a shows the tortuosity of the shortest path, L_s/d in the three regimes. For the case where $\xi_{ch} \sim O(\xi_0)$, the length of the shortest path is almost equal to the distance between the two wells. As F_N increases, the shortest path becomes more tortuous. It becomes independent of F_N when $\frac{\xi_{ch}}{R} \gg 1$ after reaching the fractal regime. Figure 7b shows the average fraction of the injection rate flowing through the shortest path, $\langle f_j\rangle_s$ for various networks stimulated at different values of F_N. As can be seen in the figure, $\langle f_j\rangle_s$ increases as the network becomes sparser when fewer tortuous paths connect the two wells. When the network becomes fractal and that there is almost one path between the two wells, most of the fluid is flowing through the shortest path.

The combined effects of M_s and τ_s lead to changes in the thermal performance of a geothermal reservoir when it is stimulated at different conditions. As seen in figure 4, the production temperature of the circulated fluid after ten years of operation decreases when the network becomes sparser and the intermediate regime is approached. In the intermediate regime, the values of M_s^{-1} and τ_s decrease

leading to increased performance of the network as it becomes sparser. In the fractal regime, the contribution of the shortest path levels off leading to a thermal performance that is independent of the value of F_N.

Now, let us elucidate the effects of network structure on the properties of the shortest path in the three regimes. The residence time of a path is proportional to its length and inversely proportional to its flow rate. In general, the length and flow rate of the shortest path increases as the connectivity of the network decreases as shown in figure 7. The length of the shortest path is increased due to two factors; the distance between the two wells and the sparsity of the network. Since the radius of the cluster increases with F_N when the volume of the injected fluid is kept constant, d increases with F_N when $\frac{d}{R}$ is kept fixed. As mentioned in section 2, the tortuosity of the shortest path increases when the cluster of activated fractures becomes sparse as shown in figure 7a. The average flow within the shortest path, $\langle f_j \rangle_s$, is proportional to Z/L_s. When the network becomes sparser, the impedance of the network increases as the number of paths decreases while their tortuosity increases and thus the average flow within the shortest path increases. As seen in the figure both, L_s and $\langle f_j \rangle_s$, increase monotonically with F_N but at different rates in the three regimes leading to the behavior observed in figure 6b.

In the homogenous regime, as F_N increases, the length of the shortest path changes slowly when compared to the changes in the average flow within it leading to a decrease in the residence time with F_N. Since the viscous pressure drop is dominant over the variability in the critical pressures in this regime, the interior of the network is more connected than the regions near the edge of the cluster since the fluid pressure is lower in that region. Changes in the viscous pressure drop hardly alter the interior connectivity of the cluster where the fluid pressure is much larger than the fracture's critical pressures. Even though the production well is placed near the edge of the cluster, i.e. $\frac{d}{R} = 0.8$, the length of the shortest path slowly changes with F_N. The average flow within the shortest path, however, changes dramatically as F_N increases. This is due to changes in the impedance of the network as the number of the paths connecting the two wells decreases as the network becomes sparser.

When the viscous pressure drop becomes comparable with the variability in the critical pressures, as the intermediate regime is reached, changes in the viscous pressure drop are felt everywhere in the network. Hence, the connectivity of the interior region of the cluster changes with F_N and the length of the shortest path increases as the viscous pressure drop during the stimulation process decreases. Since $\langle f_j \rangle_s \sim 1/L_s$, the increase in the length of the shortest path slows down the rate at which the average flow within the network increases with F_N as shown in figure 7b. Therefore, τ_s increases as the network becomes sparser reducing the contribution of the shortest path to the thermal drawdown of the geothermal reservoir. In the fractal regime, the impedance of an infinite network becomes proportional to L_s and $\langle f_j \rangle_s = 1$ since there exists only one path connecting the two wells. Since the length of the shortest path does not change with F_N in this regime, the residence time within the shortest path levels off.

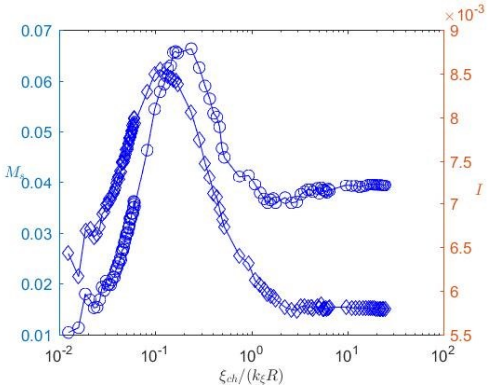

Figure 8: Comparison between changes in the values M_s and $I \equiv \frac{\langle f_j \rangle_s}{\langle \langle f_j \rangle_k \rangle} \frac{1}{N_{conv}}$ with the cluster of activated fracture's correlation length in the three growth regimes for the case of injecting 900 m^3 during the stimulation process. The circular symbols represents the values of M_s while the diamond symbols represents the values of I. The figure supports the hypothesis that $M_s \propto I$ since changes in M_s with F_N follows changes in I.

Now, let us analyze how the multiplicative term of the shortest path, M_s, changes with the network's sparsity. In section 3, it was shown that the value of M_s= 1 when the shortest path is the sole path connecting the two wells. As the path becomes interconnected with the network, M_s is expected to decrease. The value of M_s for an interconnected network, depends on both the relative average flow within the shortest path to the average flow of the other paths intersecting with it and the frequency of intersections. As the average flow within the shortest path is increased relative to the average flow within the network, M_s is increased since the fraction of the flow supplying a junction node from the segment belonging to the shortest path is increased. The frequency of intersection can be measured by the number of intersection points per the length of the shortest path, n_{conv}. $n_{conv} \equiv \frac{N_{conv}}{L_s}$ where N_{conv} where the number of segments that belong to the shortest path whose χ_j value is less than one, i.e. it supplies the fluid along with other segments from other paths to the same junction point. The frequency of intersection between the paths, n_{conv}, decreases as the network becomes sparser. In fact, it decreases monotonically as F_N increases and can be written as a function of the network's impedance, Z, figure not shown. Since $M_s = \prod_{j \in S_s} \chi_j$, it is directly proportional to N_{conv} which is a function of the intersection frequency and the length of the shortest path. Hence,

the competition between the increase in the length of the shortest path and the decrease in n_{conv} as the network becomes sparser determines the behavior of M_s. By considering both effects of the relative flow within the shortest path to the flow within the network and the frequency of the shortest path intersecting other paths, one can deduce that $M_s \propto \frac{\langle f_j \rangle_s}{\langle \langle f_j \rangle_k \rangle} \frac{1}{N_{conv}}$ where $\langle \langle f_j \rangle_k \rangle$ is the mean of the average flow within the contributing paths, i.e. $\langle \langle f_j \rangle_k \rangle = \frac{1}{n_p} \sum_k^{n_p} \frac{l}{L_k Q} \sum_{j \in S_k} q_j$. Figure 8 shows how changes in M_s with F_N follows the changes in $I \equiv \frac{\langle f_j \rangle_s}{\langle \langle f_j \rangle_k \rangle} \frac{1}{N_{conv}}$ for the case where 900 m^3 of the fracturing fluid is used to stimulate the rock.

In the homogenous regime, the length of the shortest path barely changes while the number of paths decreases. Hence, N_{conv} decreases and the average flow within the shortest path increases leading to an increase in M_s. In the intermediate regime, the length of the shortest path increases and it was shown that the average residence time within the shortest path increases. Therefore, N_{conv} is expected to decrease faster than the increase in the average flow rate within the shortest path, since $N_{conv} \sim L_s$ leading to a decrease in the multiplicative term.

5. CONCLUSION

When comparing the contribution of the flow paths to the thermal breakthrough of engineered geothermal systems that are stimulated at different process conditions, the shortest path between the injection and production wells was found to be the critical one in controlling the thermal performance of the stimulated reservoir. Specifically, the residence time within the shortest path, τ_s, and the degree of mixing between the fluid flowing through the shortest path and fluid from other paths of the network, M_s^{-1}, control the thermal performance of the stimulated reservoir. Both parameters are functions of the connectivity of the network of activated fractures measured by its characteristic correlation length, ξ_{ch}. $\xi_{ch}$is controlled by the ratio of the viscous pressure drop required to drive the injected fracturing fluid to the variability in the critical pressures required to activate the natural fractures. Three regimes were identified where the dependence of τ_s and M_s on ξ_{ch} is different: 1) a homogenous regime where the fracturing process is dominated by the viscous pressure drop forming a well-connected network, 2) a fractal regime where the viscous pressure drop is negligible and the range of the fractures' critical pressures control the fracturing process forming a fractal network with a fractal dimension of 1.9, and 3) an intermediate regime where the viscous pressure drop is important over the length scale of the cluster's radius but is negligible over ξ_0 in which a nearly fractal network is formed.

In the homogenous regime, the network connectivity and thus the thermal performance is not affected by ξ_{ch} since the viscous pressure drop dominates the activation process. As one transients from the homogenous regime to the intermediate regime, the residence time within the shortest path decreases as ξ_{ch}increases. In this regime, increasing ξ_{ch}does not affect the connectivity of the interior region within the network where the fluid pressure is much larger than the average critical pressure to activate the fractures. Hence, τ_s decreases as the length of the shortest path does not change while the average flow within it increases as the number of the paths connecting the two wells decreases. Moreover, the degree of mixing in this regime also decreases as the connectivity of the network is decreased. This is due to both the decrease in the frequency of intersection of the shortest path with other paths within the network and the increase in the average flow within the shortest path relative to the flow with other paths. Both effects combined decreases the thermal performance of the reservoirs as ξ_{ch} increases.

When the intermediate regime is fully developed, small perturbations in the value of ξ_{ch}affect the connectivity of the whole network including the interior region. In this regime, the length of the shortest path, L_s, becomes more tortuous as the network becomes sparer. The increase in the length of the shortest path with ξ_{ch} due to tortuosity is augmented by the well separation, d, which increases with the radial extent of the cluster, R. The residence time of the circulated fluid within the shortest path, though the average flow within it increases, is increased. Similarly, the degree of mixing increases although the frequency of intersection between the shortest path with the other paths decreases. This is due to the increase in the absolute number of intersections as L_s increases. As a result, the thermal performance of the network of activated fractures increases when the viscous pressure drop during the fracturing process is decreased. Similar to the homogenous regime, the thermal performance becomes independent of ξ_{ch} when the network becomes fractal. In this regime, the viscous pressure drop becomes negligible over the length scale of the cluster's radius and thus the network's topology does not change with the viscosity of the fracturing fluid or the rate at which it is injected.

Finally, more analysis is needed to provide a fuller understanding of the optimal fracturing strategies to maximize the thermal performance of an engineered geothermal system. The present model ignores the effects of the thermal interference between the activated fractures. Such effects are important when ξ_{ch} is of the same order of magnitude as the penetration depth. Therefore, the current model overpredicts the thermal performance, especially when ξ_{ch} becomes of the same order of magnitude as the average separation distance between the pre-existing fractures in the homogenous regime which we found to perform the best among other regimes. To account for the thermal interference; other numerical approaches such as continuum modeling are more suitable. Moreover, the variability in the hydraulic conductance of the fractures was ignored. Therefore, there might exists other flow paths that are longer than the shortest path which contribute more to the thermal performance. This effect can be addressed by relaxing the assumption of unified fracture apertures when they are activated. Lastly, the flow structure over the lifetime of the reservoir can change due to thermal stresses, scaling of the fracture's surfaces, etc which were ignored. Sparse networks such as the ones formed in the fractal regime are expected to be very sensitive to such physiochemical processes.

REFERENCES

Arnorsson, S., Geothermal Systems in Iceland: Structure and Conceptual Models-I. High-Temperature Areas, *Geothermics*, **24**, (1995), 561-602.

Bruel, D., Using the Migration of the Induced Seismicity as a Constraint for Fractured Hot Dry Rock Reservoir Modelling, *Inter. J. Rock Mech. and Mining Sci.*, **44**, (2007), 1106–1117.

Dokholyan, N. V., Buldyrev, S. V., Havlin, S., King, P. R., Lee, Y., and Stanley, H. E., Distribution of Shortest Paths in Percolation, *Physica A*, **266**, (1999), 55–61.

Fairley, J. P., and Hinds, J. J., Field Observation of Fluid Circulation Patterns in a Normal Fault System, *Geophys. Res. Lett.,* **31** , (2004).

Fox, D. B, Koch, D. L., and Tester, J. W., An Analytical Thermohydraulic Model for Discretely Fractured Geothermal Reservoirs, *Water Resources Res.,* **52** , (2016), 6792-6817.Kohl, T., and T. Megel, Predictive Modeling of Reservoir Response to Hydraulic Stimulations at the European EGS Site Soultz-sous-Forets, *Inter. J. Rock Mech. and Mining Sci.*, **44**, (2007), 1118-1131.

Rahman, M., Hossain, M., M., and Rahman. S. S., A Shear-Dilation-Based Model for Evaluation of Hydraulically Stimulated Naturally Fractured Resrvoirs, *Int. J. Num. Analyt. Methods Geomech.*, **26**, (2002).

Sahimi, M., Flow and Transport in Porous Media and Fractured Rocks: From Classical Methods to Modern Approaches, 2011.

Sener, M., and Gevrek,A. I., Distribution and Significance of Hydrothermal Alteration Minerals in the Tuzla Hydrothermal System, Canakkale, Turkey, *J. Volc. Geotherm. Res.*, **96**, (2000).

Tayeb, A. T, Sahimi, M., Aminzadeh F, and Sammis, C. G., Use of Microseismicity for Determining The Structure of The Fracture Network of Large-Scale Porous Media, *Phys. Rev. E*., **87**, (2013).

Tenzer, H., Development of Hot Dry Rock Technology. *GHC Bulletin*. 2001.

Wang, C., and Mao, N. H, Shearing of Saturated Clays in Rock Joins at High Confining Pressures, *Geo. Res. Lett.*, **6**, (1979), 825-828.

Willis-Richards, J., Watanabe, K., and Takahashi, H., Progress Toward a Stochastic Rock Mechanics Model of Engineered Geothermal Systems, *J. Geophys. Res*., **101**, (1996).

Zimmerman, R. W., and Bodvarsson, G. S., Hydraulic Conductivity of Rock Fractures, *Trans. Porous Media*, **23**, (1996).

Zhou, Z., Yang, J., Deng, Y., and Ziff, R. M., Shortest-Path Fractal Dimension for Percolation in Two and Three Dimensions, *Phys. Rev. E*, **86**, (2012).

APPENDIX A. VALUE OF THE PARAMETERS USED DURING THE CIRCULATION

Parameter	Value
k_r	2.9 W/m/°C
ρ_f	1000 kg/m^3
μ	1 cP
ρ_r	1050 kg/m^3
c_{p_r}	2700 J/kg/°C
c_{p_f}	4184 J/kg/°C
T_w	20 °C
T_r	200 °C
P_{inj}	20 MPa
Q	5 L/s
b	1 mm
l	20 m
H	100 m

Table 1A: Value of the parameters used during the circulation

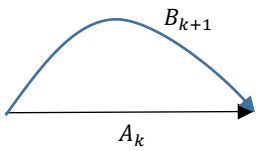

Figure 1A: This sketch shows a simple case where two paths are intersecting and how M_k depends on the interconnectivity of the network. In this sketch, a portion of path k, denoted as A_k, is intersected by another portion B from path $k+1$. In this case, the ratio of the flow within A_k to the flow within B_{k+1} will depend on their lengths. Hence, the multiplicative term, M_k, for path k will be proportional to the ratio of their lengths when the aperture and width of all the fractures are the same, i.e. $M_k \propto \frac{L_{B_{k+1}}}{L_{A_k}}$. Whenever such a situation occurs along the path of interest, M_k is multiplied by the ratio of the lengths of the portion of the intersecting paths. Therefore, the value of M_k for interconnected paths depends on the topology of the network and is difficult to approximate without further assumptions. The situation becomes even more complex when A_k and B_{k+1} do not intersect in two points. That is when B_{k+1}starts from another path other than path k.